Effect of turbostratic disorder on the staging phase diagram of lithium-intercalated graphitic carbon hosts

Tao Zheng and J. R. Dahn
Department of Physics, Simon Fraser University, Burnaby, British Columbia, Canada V5A 1S6
(Received 8 August 1995)

The staging phase transitions which occur during the intercalation of lithium in graphitic carbons were probed by *in situ* x-ray-diffraction and electrochemical methods. Turbostratic disorder (a random rotation or translation between adjacent graphene layers) in graphitic carbons (heat treated above 2200°C) affects the formation of staged phases because lithium does not insert between randomly stacked graphene layers. We call these interlayer spaces ''blocked galleries,'' which frustrate the formation of the regular sequence of full and empty galleries, characteristic of staged phases. Higher staged phases, like stage 4 and stage 3, are eliminated as the probability P for turbostratic disorder increases in graphitic carbons made at temperatures near 2300 °C. Here, a staging phase diagram is developed in the P-x plane, where x is the lithium concentration in Li_xC_6, which demonstrates how the turbostratic disorder affects staging.

INTRODUCTION

Graphite intercalation compounds represent a unique model system for the study of the ground state of a quasi-one-dimensional system. There are staged phases which form during the intercalation of lithium in graphite or graphitic carbons. Stage-n order is the periodic sequence of n graphene sheets and one lithium layer stacked along the layer normal.

The phenomenon of lithium intercalation in graphite has been known for a long time.[1] However, it is only recently that physicists and chemists have used lithium intercalation in graphite or graphitic carbons as the basis of the anode in advanced lithium-ion batteries.[2] Such lithium-ion cells are now the state-of-the-art small-size rechargeable power sources for consumer electronics. Researchers and developers of such batteries noticed that the intercalation of lithium in carbon depends on the crystal structure of the carbons.[3] Furthermore, we reported the phenomenon of ''blocked'' galleries, located between randomly stacked graphene layers, into which lithium cannot be inserted.[4] We showed previously how the presence of blocked galleries influences the staged phases and the compositions of stage-1 and stage-2 materials.[4]

Most commercialized graphitic carbons are made from soft carbon precursors. Coke-type materials are formed when the heat-treatment temperature is limited to around 1000 °C. These materials have relatively small graphene sheets of lateral extent between 20 and 50 Å. The small graphene sheets are stacked in a roughly parallel fashion, but with random rotations and translations between every pair of layers, characteristic of ''turbostratic disorder.''[5] As the carbon materials are continuously heated to 2000 °C, the lateral extent of the graphene sheets grows and the stacking becomes more parallel, as evidenced by a sharpening of the (002) Bragg peak. However, there is still complete turbostratic disorder even at this heat-treatment temperature. Upon heating above 2200 °C, the turbostratic disorder is relieved in a more or less continuous way so that by 3000 °C, synthetic graphite is produced.

Based on the concept of turbostratic disorder, Shi *et al.*[6] developed a structure refinement program for disordered carbons. The program is extremely good for studying the x-ray powder diffraction of graphitic carbons as we showed before.[3,4] The parameters of the structural model are optimized by performing a least-squares fit between the measured pattern and a theoretical calculation. For graphitic carbons, the structure is well described by two-layer packages stacked in AB registry, which are then stacked in following ways: (1) a turbostratic shift between adjacent packages with probability P'; (2) a registered shift between adjacent packages with probability P'_t, to describe local order of the type $AB/CA/BC$, etc; (3) no shift between adjacent packages to obtain the stacking sequence $AB/AB/AB$, etc., with probability $(1-P'-P'_t)$. Therefore, if $P'=0$ and $P'_t=0$, 2H graphite is obtained, and if $P'=1$ and $P'_t=0$, turbostratic graphite (50%) is obtained. It is more convenient to use the stacking probability per layer, and so we will use $P=P'/2$ and $P_t=P'_t/2$ below.

Electrochemical methods and *in situ* x-ray-diffraction measurements can help probe single- and two-phase regions during lithium intercalation in graphite and in graphitic carbons.[7,8] The structure refinement program for disordered carbon can be used to measure the turbostratic disorder probability P, and we have shown[4,8] that changes in P affect the staged phases formed during lithium intercalation. For example, we found that graphitic carbons with $P>0.3$ only showed stage-1 and stage-2 phases, while those with less turbostratic disorder showed staged phases up to stage 4.[8] Here, we concentrate on the determination of the staging phase diagram of lithium-intercalated graphitic carbons as a function of P and x in Li_xC_6 at room temperature.

EXPERIMENT

Two types of graphitic carbons were used in our study. Mesocarbon microbeads (MCMB's), were obtained from Osaka Gas Ltd. This sample had been heat treated to about 1000 °C. We used a Centorr (series 10) graphitizing furnace

TABLE I. Graphitic carbon samples studied in this work.

Sample	Heat-treatment temperature (°C)	$d_{(002)}$ (Å)	P
JMI	?	3.356	0.05
MCMB2800	2800	3.352	0.10
MCMB2700	2700	3.357	0.17
MCMB2600	2600	3.358	0.21
MCMB2500	2500	3.359	0.24
MCMB2400	2400	3.363	0.29
MCMB2300	2300	3.369	0.37

to further heat the carbons under inert gas to 2300, 2400, 2500, 2600, 2700, and 2800 °C. The soaking temperature was maintained for 1 h. These samples were then coded by their final heat treatment temperatures, MCMB2300, . . . , and MCMB2800, respectively. A commercial graphite powder labeled JMI was obtained from Johnson Matthey Inc.

Powder x-ray-diffraction measurements were made using a Siemens D5000 diffractometer equipped with a copper target tube and a diffracted beam monochromator. Well-ground powder samples were held in a rectangular well of dimensions 20 mm×12 mm ×2.1 mm in a stainless steel holder. The diffraction data were collected from 10° to 120° in scattering angle. Then we used the structure refinement program to analyze the graphitic carbons. As we discussed previously,[4,8] the calculated models fit the x-ray-diffraction patterns of graphitic carbon powders very well. The structural parameters P and $d_{(002)}$ for all the samples are listed in Table I.

Electrodes of graphitic carbons were made by coating slurries of the ground carbon powder, 5% by weight of Super S Battery Black (Chemetals Inc.) and a binder solution with 9.4% polyvinylidene fluoride dissolved in N-methyl pyrrolidinone on flat copper-foil substrates. The electrodes were dried overnight at 110 °C in air and then pressed between two flat stainless steel plates under a pressure of about 100 bars. Coin-type cells (two cells for each sample) were then made using those electrodes. The *in situ* x-ray cells of JMI, MCMB2700, and MCMB2300 were constructed by first coating the above slurries onto beryllium sheets, which were later used both as ''windows'' to x-ray beams and as the electrode current collector. The *in situ* x-ray cell design is described in Ref. 9. The electrolyte used was a 1 mol solution of $LiPF_6$ dissolved in a 25:25:50 volume percent mixture of propylene carbonate (PC), ethylene carbonate (EC), and dimethyl carbonate (DMC). This electrolyte is compatible with the silicone O rings which we used for sealing the cell.

The testing of all electrochemical coin-type cells was performed at 30.0±0.1°C. Cells were charged or discharged with constant currents stable to ±1%. The cell voltages were simultaneously logged by computer. The changes in lithium concentration in the intercalated carbons are calculated from the active mass of cathodes, the constant current supplied by the charger, and the time of current flow. Data were collected whenever the voltage of the cells, V, changed by ±0.001 V in the voltage range between 0.01 and 2.5 V.

The *in situ* cells were discharged or charged by Keithley 236 source-measure units. The cell was fixed at a voltage point, and once the current decayed to less than 100 nA, a diffraction pattern was collected. Then the cell voltage was switched to a new value. We collected the *in situ* x-ray data for the MCMB2700 and MCMB2300 samples using a Phillips diffractometer equipped with a copper target tube and a diffracted beam monochromator. The divergence slit was 0.5° and the receiving slit was 0.2 mm. Long counting times (120 s per point) were used to reduce noise and to get clear results for the superlattice peaks associated with the enlarged unit cell of the staged phases. An initial data set measured on the fresh cell was subtracted from each of the measurements of the superlattice peaks at the different voltage points to eliminate spurious peaks from the cell holder itself. In particular, the metallic lithium anode of the cell gives a peak near 36°, which can still be seen in the subtracted data. We did very careful *in situ* measurements on JMI graphite using the above Siemens D5000 diffractometer. The JMI *in situ* cell was fixed on the sample holder of the diffractometer during the whole measurement process for a period of over 3 weeks. We used 0.75° divergence and antiscatter slits and a 0.2 mm receiving slit for all *in situ* measurements on the JMI specimen.

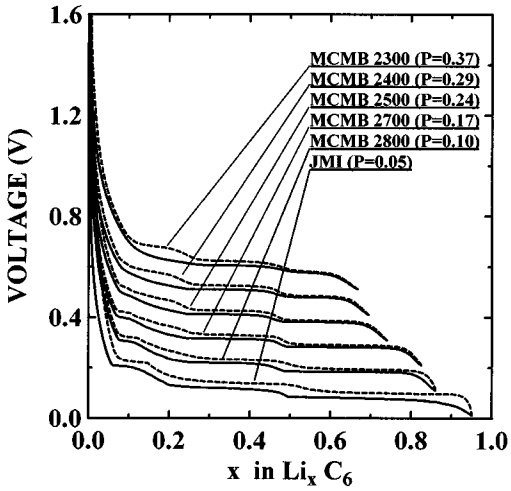

FIG. 1. Voltage profiles of the graphitic carbon samples as indicated. The curves have been shifted sequentially by 0.1 V for clarity. Solid lines are for discharge and dashed lines are for charge.

RESULTS

All electrochemical coin-type cells were tested in same manner. The first discharge-charge cycle of the cells was made with a constant current of 7.43 mA/g corresponding to a 50 h rate (a change $\Delta x = 1$ in Li_xC_6 in 50 h). A passivating film formed during the first discharge[10,11] and created about 20% irreversible capacity. Once the growth of passivating film reaches completion, the irreversible reactions apparently stop.[11]

Then a 400 h rate cycle of the cells was made using a constant current of 929 μA/g. This quasi equilibrium condition was selected for probing the staging transitions during lithium intercalation and deintercalation. Figure 1 shows the voltage profiles $V(x)$ for the second cycle of most of the graphitic carbon samples. The curves have been sequentially offset by 0.1 V for clarity. The relation between the revers-

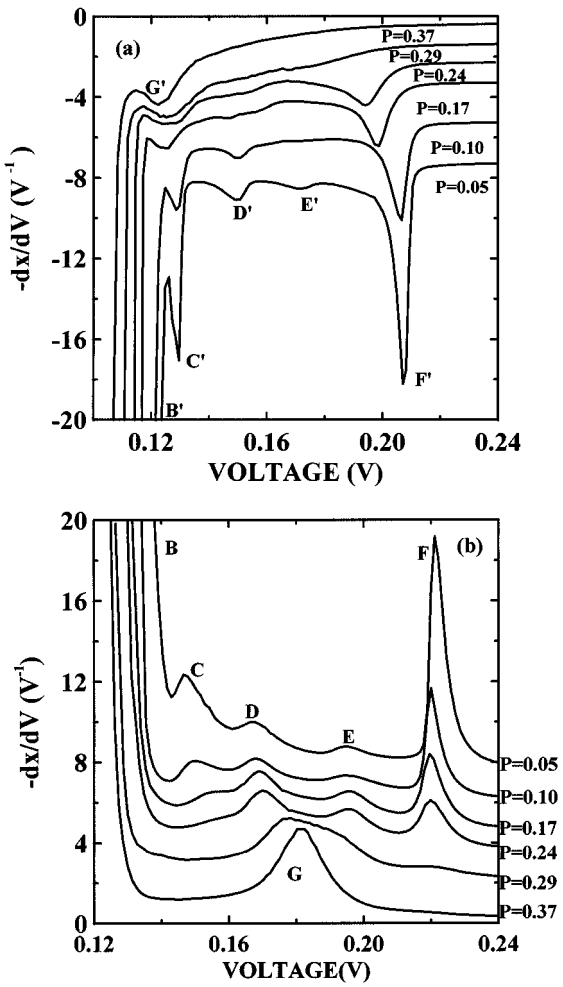

FIG. 2. Portion of the derivative $-(dx/dV)_T$ vs voltage corresponding to Fig. 1. The curves for MCMB2300, 2400, 2600, 2700, and 2800 and JMI have been sequentially shifted for clarity. The shifts are 0, -1, -2, -3, -5, and -7 V^{-1}, respectively, for the discharge shown in (a) and 0, 2, 3.5, 4.5, 6, and 7.5 V^{-1}, respectively, for the charge shown in (b). The peaks for the JMI sample have been labeled. The peaks G' and G for MCMB2300 are also labelled.

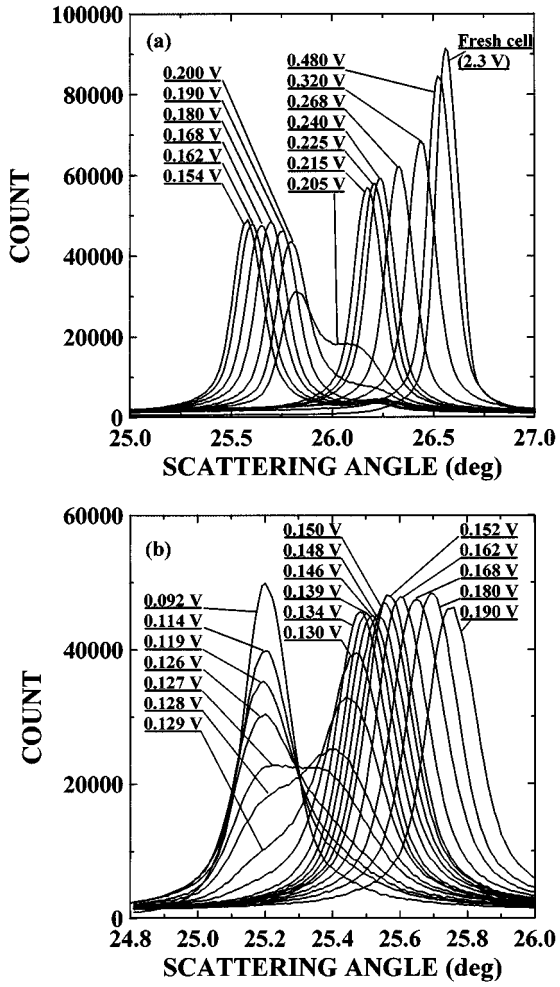

FIG. 3. *In situ* x-ray-diffraction data for the (002) Bragg peak at different voltages during the discharge of the JMI sample. The cell voltage is indicated near each scan (a) $V>0.153$ V and (b) $V<0.153$ V.

ible capacity Q and the turbostratic disorder probability P has been previously discussed.[4,8] The data are well fitted by $Q=Q_0(1-P)$ ($Q_0=372$ mA h/g corresponding to $\Delta x=1$ in Li_xC_6), which suggests no lithium intercalation in ''blocked'' galleries.[4]

The differential capacity $-(dx/dV)_T$ plotted versus V corresponding to Fig. 1 is shown in Fig. 2 for both charge and discharge. The derivative curves change continuously as P varies.[8] Peaks in $-(dx/dV)_T$ and plateaus in $V(x)$ occur at phase transitions,[7] and so once we identify the transition occurring, we can use electrochemical methods to determine the phase diagram.[12] We did *in situ* x-ray measurements on the samples JMI, MCMB2700, and MCMB2300 to understand the peaks in Fig. 2.

For the synthetic graphite sample JMI, the first *in situ* x-ray measurement was made for the fresh cell. We then equilibrated the cell at sequentially smaller voltage points in the discharge direction. One of us has reported a similar work before[7] on another synthetic graphite material KS-44 (obtained from Lonza Corporation). The JMI sample has smaller P than KS-44 ($P\approx0.10$ for KS-44), and it gives sharper features in $-(dx/dV)_T$.

Figure 3 shows the scans over the (002) Bragg peak of the JMI cell at each voltage step during the discharge (adding lithium to the sample). The (002) peak position measures the average spacing between adjacent graphene sheets. Figure 4 shows the corresponding changes in the superlattice peaks which appear between $30°\leqslant 2\theta$ (scattering angle) $\leqslant 40°$. The superlattice peak (SP) gives information about staged phases as described in Refs. 7 and 8. A summary of the changes to the (002) peak and the superlattice peaks for the JMI sample during discharge is given in Table II. Peak positions and widths were obtained by least-squares fits of pseudo-Voigt peaks to the data. The correlation lengths (CL's) were obtained by applying the Scherrer equation

$$\mathrm{CL}=0.89\lambda/(B\cos\theta),$$

where λ is the x-ray wavelength, θ is the Bragg angle, and B is the measured full width at half maximum of the superlat-

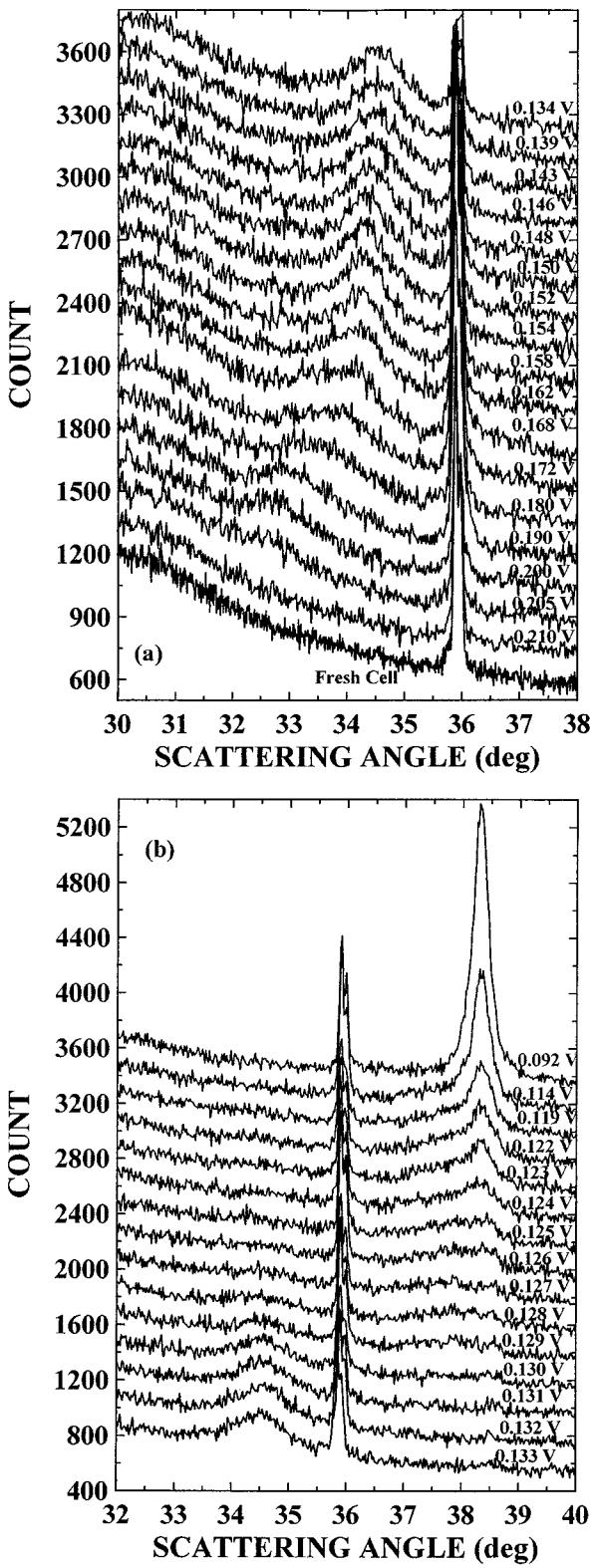

FIG. 4. *In situ* x-ray-diffraction data for the superlattice peak at different voltages for the discharge of the JMI sample. The cell voltage is indicated near each scan. The scans have been sequentially offset for clarity. (a) $V \geqslant 0.134$ V and (b) $V \leqslant 0.133$ V.

tice peaks in radians. The instrumental resolution of about $\Delta(2\theta) = 0.12°$ was not deconvoluted from the measured peak widths.

When lithium was intercalated into JMI graphite above the first plateau in Fig. 1 (corresponding to peak F' in Fig. 2), the (002) peak shifts smoothly towards smaller angle and no superlattice peaks are observed. As we reported previously,[7,8] this corresponds to a single-phase region and lithium, at low concentration, is uniformly intercalated between all the graphene sheets. We call this region the dilute stage-1 ($1'$) phase.

In an attempt to consolidate the information contained in Figs. 2, 3, and 4 for the JMI sample, we plot the differential capacity, the (002) peak position, the observed superlattice peak position, and correlation length of the staged structure versus cell voltage in Figs. 5(a)–5(d), respectively. Also plotted in Fig. 5(c) are the expected superlattice peak positions for the (005) peak from a stage-4 phase, the (004) peak from a stage-3 phase, and the (003) peak from a stage-2 phase. These expected positions are derived from the (002) peak position $2\theta_{(002)}$, using the equations

$$2\theta_{005} = 2\sin^{-1}\left[\frac{5}{4}\sin\left(\frac{(2\theta_{002})}{2}\right)\right], \tag{1}$$

$$2\theta_{004} = 2\sin^{-1}\left[\frac{4}{3}\sin\left(\frac{(2\theta_{002})}{2}\right)\right], \tag{2}$$

and

$$2\theta_{003} = 2\sin^{-1}\left[\frac{3}{2}\sin\left(\frac{(2\theta_{002})}{2}\right)\right]. \tag{3}$$

By comparing the measured superlattice peak position with those expected for the stage-4, stage-3, and stage-2 phases, we can determine which phases are present.

The superlattice peak indicating staged phases first appears below peak F' in Fig. 5(a). At 0.200 V, the peak is close to the position expected for the pure stage 4. However, Table II shows that the lithium composition is only $x = 0.118$ at this voltage, not $x = 0.25$ as expected for a filled stage-4 phase. As the voltage decreases further, the superlattice peak and the (002) peak shift continuously. At 0.180 V, the superlattice peak moves between the positions expected for pure stage-4 and stage-3 phases. So it is believed that peak F' corresponds to a transition from the stage-$1'$ phase to a mixed staged phase which includes both stage-4 and stage-3 orders. At 0.154 V, the superlattice peak is near the position expected for the pure stage 3. Between 0.180 and 0.154 V, the material is best described as a mixed staged phase, containing regions of galleries hosting lithium separated by two or three empty galleries. Apparently, the transition from stage 4 mixed with stage 3, near 0.180 V to stage 3, near 0.154 V is continuous. This may be caused by the presence of some turbostratic disorder ($P = 0.05$) in this sample.

Near 0.154 V, the correlation length of the staged phase shows a maximum [Fig. 5(d)]. This coincides with the point where the superlattice peak position matches that expected for the pure stage 3. The lithium concentration at this point is $x = 0.172$ from Table II, not $x = 0.333$ expected for a filled stage-3 phase. As the voltage decreases to 0.130 V, the superlattice peak remains near the position expected for the stage-3 phase, but continues to shift slightly above the expected position for stage 3. This is due to an admixture of

TABLE II. Summary of superlattice peaks for JMI during discharge.

Voltage (V)	x in Li_xC_6	(002) position[a] (±0.02°)	HWHM[c] of (002) peak	Stage 4L (005) expected (±0.05°)	Stage, 3L (004) expected (±0.05°)	Stage 2L or 2 (003) expected (±0.05°)	Observed SP[d]	HWHM of observed SP	CL[e] of staged order (Å)	n[f]
0.225	0.060	26.21°	0.08°							
0.215	0.064	26.18°	0.08°							
0.210	0.068	26.10°	0.09°							
0.205	0.104	26.08°, 25.82°	0.18°, 0.09°							
0.200	0.118	25.80°	0.09°	32.41°			32.78° ± 0.02°	0.61°	67	3.79
0.190	0.133	25.76°	0.09°	32.36°			33.08° ± 0.02°	0.59°	69	3.61
0.180	0.144	25.70°	0.09°	32.28°	34.50°		33.57° ± 0.03°	0.70°	59	3.35
0.168	0.158	25.65°	0.09°	32.22°	34.43°		34.00° ± 0.03°	0.90°	46	3.15
0.162	0.164	25.61°	0.09°	32.17°	34.38°		34.16° ± 0.20°	0.67°	61	3.08
0.154	0.172	25.58°	0.09°		34.34°		34.28° ± 0.02°	0.48°	86	3.02
0.152	0.175	25.57°	0.09°		34.32°		34.30° ± 0.02°	0.49°	84	3.01
0.148	0.181	25.54°	0.09°		34.28°		34.42° ± 0.02°	0.51°	81	2.95
0.146	0.184	25.52°	0.09°		34.25°		34.46° ± 0.02°	0.55°	75	2.93
0.139	0.192	25.51°	0.09°		34.24°		34.55° ± 0.02°	0.57°	72	2.90
0.134	0.197	25.49°	0.09°		34.21°		34.56° ± 0.02°	0.62°	66	2.89
0.132	0.200	25.48°	0.09°		34.20°		34.58° ± 0.02°	0.61°	67	2.88
0.130	0.210	25.47°	0.10°		34.19°		34.58° ± 0.02°	0.57°	72	2.87
0.129	0.216	25.45°,	0.12°		34.16°		34.58° ± 0.02° for (004)	0.82°	50	2.86
		25.21° (TP)[b]	0.11°			38.21°	37.8° ± 0.5° for (003)	1.5 ± 0.5°	27	2.07
0.128	0.225	25.41°,	0.14°		34.10°		34.57° ± 0.02° for (004)	0.88°	47	2.85
		25.19° (TP)	0.10°			38.18°	37.8° ± 0.5° for (003)	1.5 ± 0.5°	27	2.06
0.127	0.230	25.37°,	0.16°		34.05°		34.53° ± 0.04° for (004)	0.81°	51	2.84
		25.18° (TP)	0.10°			38.17°	37.8° ± 0.03° for (003)	1.5 ± 0.5°	27	2.06
0.126	0.234	25.19°	0.09°			38.18°	38.21° ± 0.03°	0.49°	85	2.00
0.119	0.338	25.20°	0.08°			38.20°	38.32° ± 0.02°	0.16°	260	1.98
0.114	0.418	25.20°	0.08°			38.20°	38.32° ± 0.02°	0.16°	260	1.98
0.092	0.479	25.20°	0.08°			38.20°	38.32° ± 0.02°	0.16°	260	1.98

[a]Corrected for off-axis displacement of the cell electrode.
[b]Two (002) peaks merged.
[c]Half width at half maximum.
[d]Superlattice peak.
[e]Correlation length.
[f]Stage number predicted by $2\theta_{(002)}$ and $2\theta_{(SP)}$.

some stage-2 units within the predominantly stage-3 material. At 0.130 V, the composition is $x = 0.210$.

Why is the composition of the pure stage-3 phase so different from $x = 0.333$? The sites available for lithium within a gallery form a two-dimensional triangular lattice with a lattice spacing, $a \approx 2.45$ Å. However, at ambient temperature and pressure, lithium ions cannot occupy nearest-neighbor sites because of the Coulomb repulsion between them. Thus the composition of a gallery is limited to 1/3 of the total number of sites. The triangular lattice gas with large repulsive nearest-neighbor interactions is appropriate to describe the ordering which occurs in this system. For compositions less than 1/4 (at any temperature), the atoms randomly occupy sites on each of the three $\sqrt{3}a \times \sqrt{3}a$ superlattices, but for compositions larger than 1/4, they are found predominantly on one superlattice at low temperature.[12,13] We designate the random occupation of all superlattices as a liquidlike or L phase, like stage 4L, while the preferential occupation of one superlattice is designated as a ''solid'' phase like stage 3 or stage 2. For stage 4, we expect a liquidlike phase for values of x in Li_xC_6 less than 3/16, for stage 3, we expect a liquidlike phase for x less than 1/4, and for stage 2 we expect liquidlike phases for x less than 3/8.

Based on the argument above, the stage-4, the mixed stage-3 and stage-4, and the stage-3 phases are expected to have the lithium randomly occupying the three superlattices

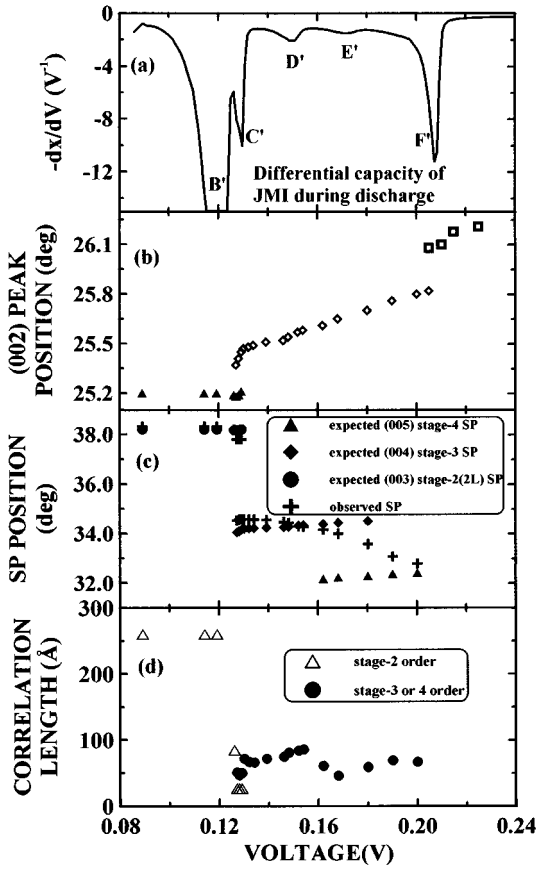

FIG. 5. (a) Differential capacity, (b) the (002) peak position, (c) the observed superlattice peak position and the expected superlattice peak positions for different staged phases as indicated, and (d) the correlation length of the staged phases plotted as a function of cell voltage for JMI graphite, respectively.

within each occupied gallery. Therefore, the region between 0.180 and 0.154 V will be called the mixed stage-4L and stage-3L region, with predominantly stage 3L at 0.154 V. The region of peak F' with voltage between 0.213 and 0.180 V corresponds to the transition from stage 1′ to the above mixed phase. Although it is tempting to assign peak D' in Fig. 5(a) to the stage-3L to stage-3 transition, this is unlikely because the composition only reaches about $x=0.200$ at 0.132 V, below peak D' and above peak C'. Based on the arguments above, we do not believe the solid stage-3 phase forms. The origin of peaks E' and D' are unknown.

As the cell voltage further decreases, peak C' is encountered. Here, a two phase region is clearly observed, where stage-3L and stage-2L phases coexist over a range of x. Figures 5(b), 5(c), and 5(d) show that for three closely spaced voltages, peaks for the two phases could be simultaneously observed. Finally, the peak B' is encountered, which is thought to correspond to the transition from the stage-2L phase to the solid stage-2 phase.[7] The position of the superlattice peak is consistent with this interpretation.

The differential capacity of the MCMB2800 sample ($P=0.10$) in Fig. 2 shows similar characteristics compared to the JMI sample, except the peaks corresponding to phase transitions are weaker. The synthetic graphite material, KS-44 with a similar P, was studied carefully before,[7] and we will incorporate those results in the staging phase diagram in the P-x plane.

We next consider the results of *in situ* x-ray measurements during the charge of the MCMB2700 sample ($P=0.17$). Table III gives the measured (002) and superlattice peak positions and half widths versus cell voltage and lithium concentration x. The expected superlattice peak positions are also given. Figures 6(a) and 6(b) show the superlattice peak as a function of cell voltage, and Fig. 7 consolidates all the information for the MCMB2700 sample, just as Fig. 5 did for JMI graphite. We can now clearly observe many of the effects of increased P. Even though the data in Figs. 6 and 7 are for the charge of the cell, we start our description from high voltage, as we did for the JMI sample.

Above peak F, there is no evidence for superlattice peaks and the material is in the stage-1′ phase. Peak F corresponds to a transition from a staged phase to the stage-1′ phase. Figure 7(c) shows that the phases at 0.216 V are coexisting stage-1′ and mixed stage-3L, stage-4L phases. For this sample, the mixed stage-3L, stage-4L phase has more stage-3L character than stage 4L. As the voltage decreases below 0.216 V, the superlattice peak moves toward the position of pure stage 3, which is reached near 0.187 V. Below 0.187 V, the superlattice peak shows a small amount of stage-2L character mixed with stage-3L character, since its position is above the angle expected for pure stage 3L. The sharp peak encountered near 0.166 V during the charge in Fig. 7(a), corresponds to the transition from stage 2L to a phase predominantly made up of stage 3L. This is clearly shown by the behavior of the superlattice peak in this voltage range in Fig. 7(c). Finally, peak B corresponds to the solid stage-2 to liquidlike stage-2L transition.

The correlation length of the staged phases is always less than 80 Å, even in the solid stage-2 phase. By contrast, the correlation length of the solid stage-2 phase for the JMI sample was at least 250 Å. Presumably this difference is caused by the increased number of blocked galleries which are present in the MCMB2700 sample compared to the JMI graphite.

Table III and Fig. 7(b) show that the (002) peak moves smoothly for the MCMB2700 sample. There are no voltages or compositions where coexisting phases with different (002) plane spacings are observed. Instead, the width of the (002) peak increases slightly in those regions where coexisting phases with different (002) spacings were observed for the JMI sample. These increases in (002) peak width occur near peak F (near 0.22 V) and near the sharp peak in Fig. 7(a) at 0.166 V.

One major difference between the MCMB2700 and JMI samples is that the former shows no superlattice peak for a pure stage-4L order. However, the peaks F in Fig. 2 for samples JMI and MCMB2700 are similar in shape, although the peak for MCMB2700 is reduced in intensity compared to the peak for the JMI sample. Peaks F and F' correspond to a transition between a mixed stage-3L, stage-4L phase and a dilute stage-1 phase. The proportion of stage-4L sequences in the mixed staged phase is reduced as P increases, which apparently weakens the strength of the transition. We expect increases in the number of blocked galleries to frustrate the formation of higher stages before lower stages. The blocked galleries can interfere with the sequence of full and empty galleries by being positioned where a full gallery is needed. Since the interactions which cause the formation of the

TABLE III. Summary of superlattice peaks for MCMB2700 during charge.

Voltage (V)	x in Li_xC_6	(002) position[a] ($\pm 0.05°$)	HWHM[b] of (002) peak	Stage $4L$ (005) expected ($\pm 0.05°$)	Stage $3L$ (004) expected ($\pm 0.05°$)	Stage $2L$ or 2 (003) expected ($\pm 0.05°$)	Observed SP[c]	HWHM of observed SP	CL[d] of staged order (Å)	n[e]
0.239	0.066	26.26°	0.14°							
0.233	0.068	26.24°	0.14°							
0.228	0.071	26.23°	0.15°							
0.224	0.076	26.19°	0.18°							
0.219	0.095	26.01°	0.17°							
0.216	0.103	25.99°	0.15°	32.65°			33.98° ± 0.02°	2.02°	20	3.34
0.213	0.107	25.87°	0.14°	32.50°	34.73°		33.98° ± 0.02°	1.16°	35	3.27
0.204	0.119	25.85°	0.14°	32.47°	34.70°		34.03° ± 0.03°	1.15°	36	3.24
0.199	0.125	25.83°	0.14°	32.45°	34.68°		34.25° ± 0.03°	1.18°	35	3.15
0.199	0.125	25.83°	0.14°	32.45°	34.68°		34.25° ± 0.03°	1.18°	35	3.15
0.192	0.140	25.78°	0.14°	32.38°	34.61°		34.54° ± 0.02°	1.02°	40	3.02
0.187	0.150	25.70°	0.14°		34.50°		34.59° ± 0.02°	0.80°	51	2.97
0.177	0.169	25.65°	0.14°		34.43°		34.79° ± 0.02°	0.74°	56	2.88
0.173	0.177	25.61°	0.15°		34.38°		35.00° ± 0.02°	0.62°	67	2.80
0.170	0.185	25.56°	0.16°		34.31°		35.07° ± 0.02°	0.71°	58	2.76
0.166	0.200	25.44°	0.17°		34.15°		35.09° ± 0.02° for (004)	1° to 2°	27,	2.71
						38.57°	38.28° ± 0.05° for (003)	1° to 2°	28	2.04
0.160	0.215	25.36°	0.16°		34.04°	38.45°	38.13° ± 0.02°	0.08°	52	2.05
0.156	0.224	25.35°	0.15°		34.02°	38.43°	38.06° ± 0.02°	0.75°	55	2.06
0.151	0.233	25.29°	0.14°		33.94°	38.34°	38.07° ± 0.02°	0.70°	59	2.04
0.145	0.244	25.27°	0.13°		33.91°	38.31°	38.03° ± 0.02°	0.64°	59	2.04
0.134	0.287	25.25°	0.13°		33.89°	38.28°	38.06° ± 0.02°	0.61°	68	2.03
0.130	0.361	25.28°	0.13°			38.32°	38.33° ± 0.02°	0.60°	69	2.00
0.128	0.424	25.30°	0.13°			38.35°	38.37° ± 0.04°	0.60°	69	2.00
0.120	0.469	25.29°	0.13°			38.34°	38.43° ± 0.02°	0.54°	77	1.99
0.093	0.540	25.25°	0.17°			38.28°	38.51° ± 0.20°	0.63°	66	1.97

[a]Corrected for off-axis displacement of the cell electrode.
[b]Half width at half maximum.
[c]Superlattice peak.
[d]Correlation length.
[e]Stage number predicted by $2\theta_{(002)}$ and $2\theta_{(SP)}$.

staged phases become weaker with stage number,[14] the blocked galleries will frustrate the higher stages first. We believe this is why the superlattice peak for pure stage-$4L$ order is absent for MCMB2700, even though it is present for the JMI sample.

In Fig. 2, the differential capacity of the MCMB2600 sample ($P=0.24$) is similar to that of the MCMB2700 sample. Though the phase transition peaks tend to be weaker and broader for the MCMB2600 sample, the positions of the peaks are coincident. We believe that the phase transitions are similar for both samples. As P increases, peaks C',D',E',F' and peaks C,D,E,F vanish, while new peaks G' and G appear, respectively, in the discharge and charge for samples heated at 2400 and 2300 °C. This emphasizes that the attributes of materials heated at 2400 and 2300 °C are different from those of graphitic carbons heated at higher temperatures. The MCMB2300 sample with $P=0.37$ has similar but sharper features compared with MCMB2400 ($P=0.29$). We decided to study the MCMB2300 sample next, and the results are presented in Table IV. Figure 8 shows *in situ* x-ray-diffraction scans over the region of the superlattice peak as the voltage of the cell was stepped sequentially upward. Figure 9 shows $-(dx/dV)$, the (002) peak position, the superlattice peak position, and the correlation length of the staged phase as a function of voltage. Figure 9(c) also shows the expected (003) superlattice peak position of the stage-2 or stage-$2L$ phase.

Figure 9(a) shows that $-(dx/dV)$ differs dramatically from that for JMI or MCMB2700. Figures 8 and 9(c) show that peak G corresponds to a transition from a stage-$2L$ phase to a stage-$1'$ phase. The transition appears continuous, because the (002) peak moves smoothly and the superlattice peak intensity vanishes smoothly. However, we believe the transition is really a first-order one broadened by disorder, because the peaks G and G' in Fig. 2 show large hysteresis in voltage. This hysteresis would not be expected for a continuous transition.

Peak B for MCMB2300 is again consistent with a transi-

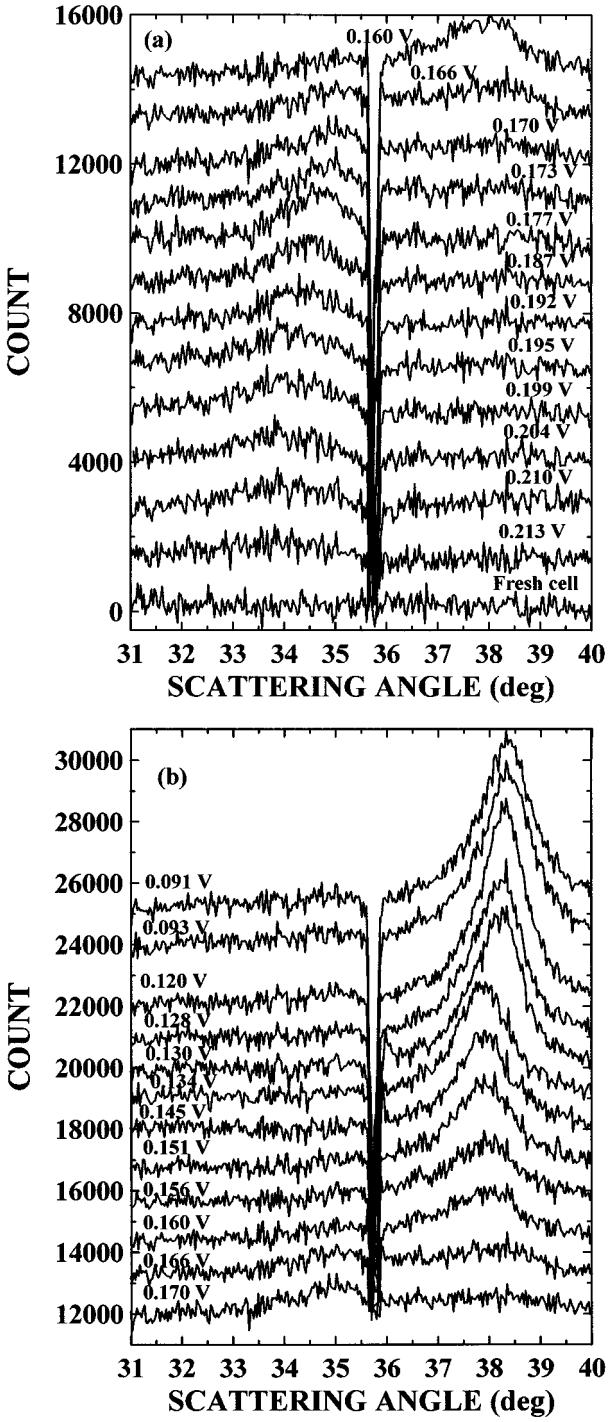

FIG. 6. *In situ* x-ray-diffraction results for the superlattice peak at different voltages as indicated for the charge of the MCMB2700 sample. (a) $V \geqslant 0.160$ V and (b) $V \leqslant 0.170$ V. The scans have been sequentially offset for clarity.

tion between phases with predominantly stage-2 character. We identify it with the solid stage-2 to liquidlike stage-2L transition.

The correlation lengths in Fig. 9(d) are even smaller than those for the MCMB2700 sample. The maximum correlation lengths appear when the superlattice peak is closest to the position expected for pure stage 2.

To understand the phase transitions which occur during the intercalation of lithium in graphitic carbon samples, we

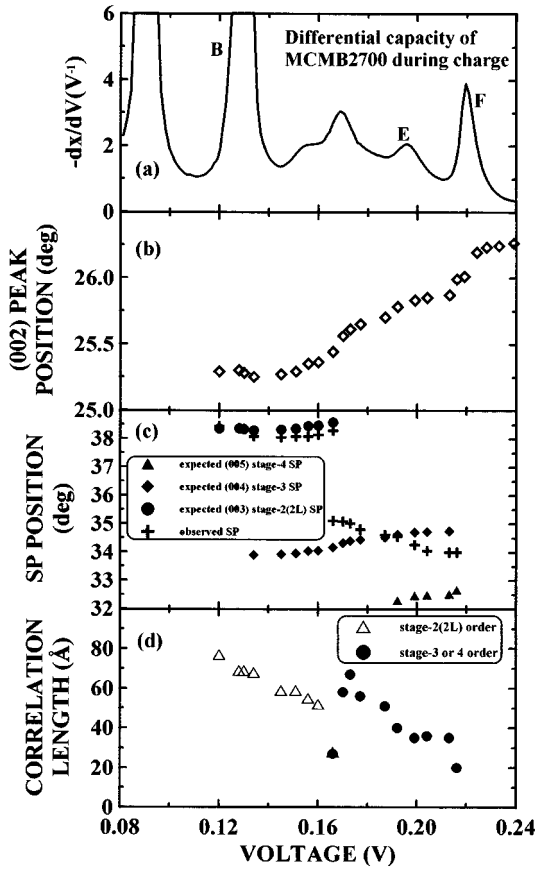

FIG. 7. (a) Differential capacity (b) the (002) peak position, (c) the observed superlattice peak position and the expected superlattice peak positions for different staged phases as indicated, and (d) the correlation length of the staged phases plotted as a function of cell voltage for the MCMB2700 sample, respectively.

consider the variation of the average stage number n as a function of x in $\mathrm{Li}_x\mathrm{C}_6$. The average stage number is defined here by

$$\frac{n+1}{n} d_{(\mathrm{SP})} = d_{(002)} . \tag{4}$$

Solving for n, we obtain

$$n = \frac{\sin(\theta_{(002)})}{\sin(\theta_{(\mathrm{SP})}) - \sin(\theta_{(002)})}, \tag{5}$$

where the subscripts (SP) and (002) correspond to the observed superlattice and (002) peaks, respectively. Therefore n can be calculated for the positions of the observed (002) and superlattice peaks. The average stage numbers for the JMI sample measured during discharge and for the MCMB2700 and MCMB2300 samples measured during charge have been calculated and are listed in Tables II, III, and IV, respectively. Figure 10 shows n versus x for JMI during discharge and MCMB2700 and MCMB2300 during charge. For JMI, the superlattice peak begins to appear with n approximately equal to 3.79, which means that the stage-$1'$ phase coexists with a staged phase with predominantly stage-4L order. This is consistent with what we had described earlier above. Then n changes in a more or less

TABLE IV. Summary of superlattice peaks for MCMB2300 during charge.

Voltage (V)	x in Li_xC_6	(002) position[a] ($\pm0.02°$)	HWHM[b] of (002) peak	stage $2L$ or 2 (003) expected ($\pm0.03°$)	Observed SP[c] ($\pm0.03°$)	HWHM of observed SP	CL[d] of staged order (Å)	n[e]
0.238	0.090	26.15°	0.16°					
0.208	0.106	26.01°	0.16°					
0.188	0.134	25.83°	0.17°					
0.177	0.183	25.55°	0.18°	38.74°	37.81°	3.18°	13	2.15
0.167	0.213	25.41°	0.16°	38.53°	38.04°	1.21°	34	2.08
0.160	0.225	25.35°	0.16°	38.43°	38.11°	1.24°	34	2.05
0.150	0.239	25.32°	0.15°	38.38°	37.91°	0.97°	43	2.07
0.136	0.258	25.31°	0.15°	38.37°	37.98°	1.16°	36	2.06
0.120	0.405	25.26°	0.15°	38.29°	38.76°	1.66°	25	1.93
0.100	0.477	25.24°	0.15°	38.26°	38.92°	1.36°	31	1.91
0.078	0.577	24.97°	0.21°					
0.049	0.635	24.83°	0.19°					

[a]Corrected for off-axis displacement of the cell electrode.
[b]Half width at half maximum.
[c]Superlattice peak.
[d]Correlation length.
[e]Stage number predicted by $2\theta_{(002)}$ and $2\theta_{(SP)}$.

smooth way as x in Li_xC_6 increases up to $x\approx0.210$. Then n changes from 3 to 2 when the transition between stage-$3L$ and stage-$2L$ phases occurs. The stage number stays at about $n=2$ during the transition from stage $2L$ to stage 2. One difference between the JMI and MCMB2700 samples is that the latter first begins to show a superlattice peak with $n=3.34$, much smaller than $n\approx3.8$ for the JMI sample. This corresponds to the mixed stage-$3L$, stage-$4L$ order. Then n decreases smoothly to near $n\approx2.7$ and the transition to stage $2L$ occurs. For MCMB2300, the stage number at $x=0.183$ during charge is larger than 2, and then it continuously decreases to slightly below 2 as x increases. Stage-$2L$ and stage-2 orders are predominant in the MCMB2300 sample.

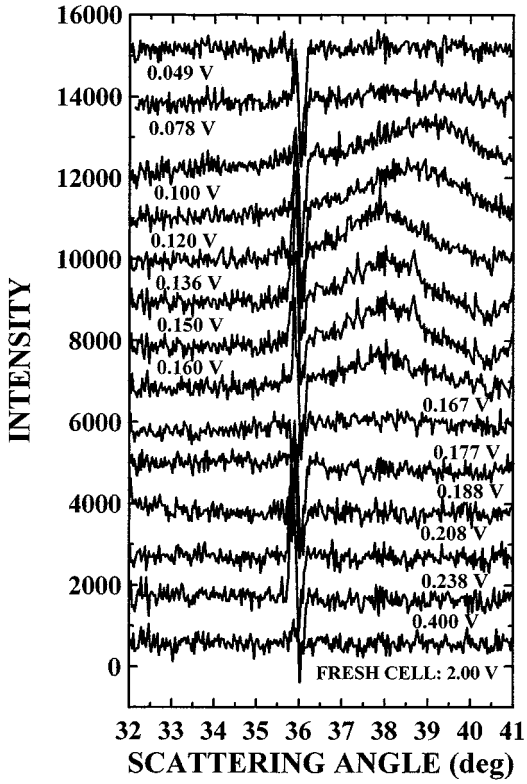

FIG. 8. *In situ* x-ray-diffraction results for the superlattice peak at different voltages during the charge of the MCMB2300 sample. The scans have been sequentially offset for clarity.

SUMMARY

It is now possible to summarize the effects of increases in P on the staged phases which form in lithium-intercalated graphite. As P increases, higher stages are eliminated first. Based on the electrochemical data in Fig. 2, for $P\geqslant0.30$, peaks F and F' are eliminated and the mixed staged phase (stage $3L$, stage $4L$) no longer forms. For higher, P, peaks G and G' are formed and only the stage-1, stage-2, stage-$2L$, and dilute stage-1 phases exist. The correlation length of the staged sequence decreases as P increases, as we expected.

Figure 11 shows our attempt to place this information on a staging phase diagram for Li_xC_6 in the P-x plane at room temperature. Figure 11(a) is for samples produced as lithium is intercalated (discharge), and Fig. 11(b) is for samples produced as lithium is removed (charge). The electrochemical information in Figs. 1 and 2 and the *in situ* x-ray-diffraction data presented throughout this paper have been used to construct this diagram, as described below.

The peaks in the differential capacity curves in Fig. 2 represent coexisting phases. For the discharge (Fig. 2), the first point where dx/dV near peak F' begins to deviate from the background is the end point of the pure stage-$1'$ phase. The phase labeled M represents the mixed stage-$3L$, stage-$4L$ phase. The area under peak F' during discharge or F during charge is the width of the stage-$1'-M$ coexistence region. The single-phase regions of stage-$2L$, stage-2, and

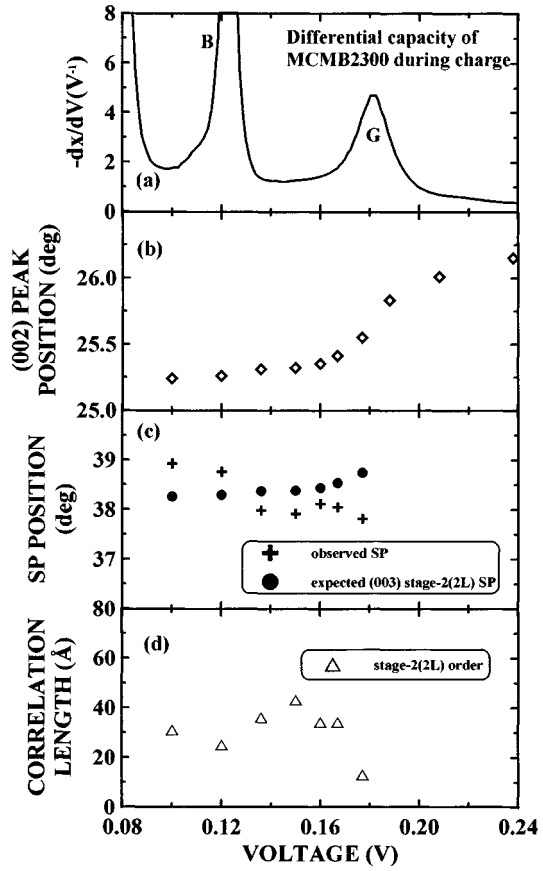

FIG. 9. (a) Differential capacity, (b) the (002) peak position, (c) the observed superlattice peak position and the expected superlattice peak position for a stage-2 or stage-2L phase, and (d) the correlation length of the staged phase plotted as a function of cell voltage for the MCMB2300 sample, respectively.

stage-1 phases are narrow and of maximum width $\Delta x = 0.03$; these are denoted as heavier lines in Fig. 11. The x positions of these single phases are determined from the compositions corresponding to the minima in dx/dV between peaks corresponding to coexisting phases in Fig. 2. The minimum point at the left base of peaks F or F' in Fig. 2 gives the low-x composition of the M phase. Peaks C and C' correspond to a phase transition between phase M and stage $2L$. So their area can be used to extract the width of the two-phase regions. The minimum point between peaks C and B or C' and B' corresponds to the composition of the line phase of stage $2L$. By considering the compositions of the positions of the minima in dx/dV and the area of the peaks in dx/dV in this way, the phase diagram can be determined. Data from Ref. 7 were used to identify the peaks in MCMB2800, which has a similar P to KS-44.

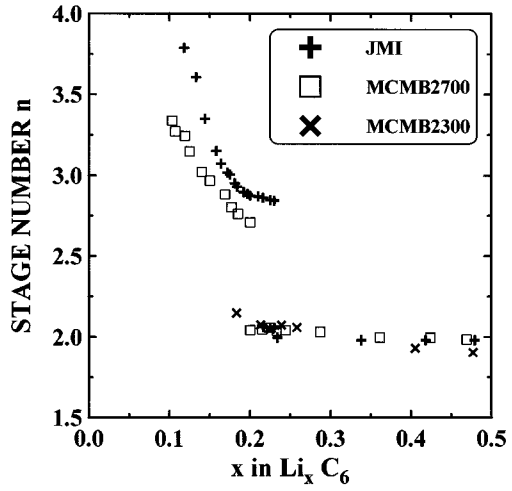

FIG. 10. Average stage number n plotted as a function of x in Li_xC_6 for the JMI sample during discharge and for MCMB2700 and MCMB2300 samples during charge, respectively.

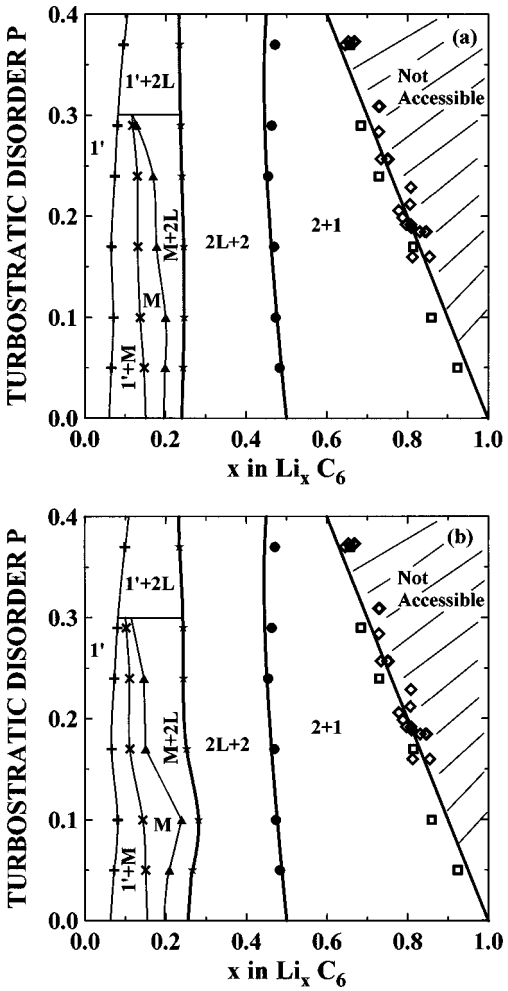

FIG. 11. Phase diagram for lithium-intercalated graphitic carbon in the P-x plane. (a) Discharge and (b) charge. All symbols are from the results of electrochemical or *in situ* x-ray measurements. The M phase is the mixed stage-3L, stage-4L phase. The stage-2L, stage-2, and stage-1 phases are depicted as line phases here (thick lines), although they have some small range of x. The solid lines are guides to the eye.

When P is small ($P \leqslant 0.10$), the transition from stage $1'$ to M is to a phase which is predominantly stage $4L$. As P increases, the amount of stage $3L$ in this phase increases. Eventually, even stage $3L$ cannot form (near $P = 0.3$) and the mixed staged phase M vanishes for $P > 0.3$.

The shaded region at the right-hand side of the diagram represents compositions that cannot be prepared because lithium cannot be inserted into ''blocked'' galleries. The data

that define this region come from Ref. 4.

Figure 11 shows a phase diagram which a meaningful theory of lithium intercalation in graphite must be able to reproduce. Turbostratic disorder is present in most synthetic graphites and hence affects experimental results. Furthermore, the voltage and $-(dx/dV)$ profiles in Figs. 1 and 2 must also be replicated by any theory considered to be viable. At the moment, all existing phenomenological theories for lithium intercalation in graphite cannot reproduce the experimental results shown here.

[1] A. Herold, Bull. Soc. Chim. France **187**, 999 (1955); R. Juza and V. Wehle, Nature (London) **52**, 560 (1965); J. E. Fischer and H. J. Kim, Synth. Met. **12**, 137 (1985).
[2] T. Nagaura and K. Tozawa, Prog. Batteries Sol. Cells **9**, 209 (1990).
[3] J. R. Dahn, A. K. Sleigh, Hang Shi, J. N. Reimers, Q. Zhong, and B. M. Way, Electrochim. Acta **38**, 1179 (1993).
[4] Tao Zheng, J. N. Reimers, and J. R. Dahn, Phys. Rev. B **51**, 734 (1995).
[5] B. E. Warren, Phys. Rev. B **9**, 693 (1941).
[6] Hang Shi, J. N. Reimers, and J. R. Dahn, J. Appl. Crystallogr. **26**, 827 (1993).
[7] J. R. Dahn, Phys. Rev. B **44**, 9170 (1991).
[8] Tao Zheng and J. R. Dahn, Synth. Met. **73**, 1 (1995).
[9] J. R. Dahn, M. A. Py, and R. R. Haering, Can. J. Phys. **60**, 307 (1982).
[10] E. Peled, J. Electrochem. Soc. **126**, 2047 (1979).
[11] R. Fong, U. von Sacken, and J. R. Dahn, J. Electrochem. Soc. **137**, 2009 (1990).
[12] A. J. Berlinsky, W. G. Unruh, W. R. Mckinnon, and R. R. Haering, Solid State Commun. **31**, 135 (1979).
[13] M. Schick, J. S. Walker, and M. Wortis, Phys. Rev. B **16**, 2205 (1977).
[14] S. A. Safran, Phys. Rev. Lett. **44**, 937 (1980).